Japanese Journal of Applied Physics



RAPID COMMUNICATION

# Electrical properties of unintentionally doped $\beta$-$Ga_2O_3$ (010) thin films grown by a low-pressure hot-wall metalorganic chemical vapor deposition

Japanese Journal of Applied Physics **63**, 080901 (2024) **RAPID COMMUNICATION**
https://doi.org/10.35848/1347-4065/ad6542

# Electrical properties of unintentionally doped $\beta$-$Ga_2O_3$ (010) thin films grown by a low-pressure hot-wall metalorganic chemical vapor deposition

Jun Jason Morihara[1], Jin Inajima[1], Zhenwei Wang[2], Junya Yoshinaga[3,4], Shota Sato[1], Kohki Eguchi[1], Takuya Tsutsumi[1], Yoshinao Kumagai[3], and Masataka Higashiwaki[1,2*]

[1]*Department of Physics and Electronics, Osaka Metropolitan University, Sakai, Osaka 599-8531, Japan*
[2]*National Institute of Information and Communications Technology, Koganei, Tokyo 184-8795, Japan*
[3]*Department of Applied Chemistry, Tokyo University of Agriculture and Technology, Koganei, Tokyo 184-8588, Japan*
[4]*TAIYO NIPPON SANSO CORPORATION, Yokohama, Kanagawa 220-8561, Japan*

*E-mail: sj24817v@st.omu.ac.jp; higashiwaki@omu.ac.jp

Received July 5, 2024; revised July 14, 2024; accepted July 18, 2024; published online August 6, 2024

We investigated the electrical properties of unintentionally doped (UID) $Ga_2O_3$ (010) layers grown by low-pressure hot-wall metalorganic chemical vapor depositions from device characteristics of Schottky barrier diodes (SBDs) fabricated on them. Highly resistive properties of the UID $Ga_2O_3$ layers were confirmed from current–voltage characteristics. The specific on-resistance of the SBD with the most resistive UID $Ga_2O_3$ layer was $2.2 \times 10^7$ Ωcm$^2$. Capacitance–voltage characteristics revealed that most of the SBDs had complete depletion of the UID layers at thermal equilibrium, indicating that their residual effective donor densities were less than $3.0 \times 10^{13}$ cm$^{-3}$. 

$\beta$-$Ga_2O_3$ has been attracting a great deal of interest as a next-generation semiconductor material owing to its superior material properties such as a large bandgap energy of 4.5 eV,[1)] a large breakdown electric field of over 7 MV cm$^{-1}$,[2–4)] and controllable $n$-type conductivity in a wide range of electron density by intentional donor doping.[5–7)] The breakdown electric field leads to a large Baliga's figure of merit of $\beta$-$Ga_2O_3$,[8)] which is several times larger than those of SiC and GaN. Another important material feature of $\beta$-$Ga_2O_3$ is that bulk single crystals can be synthesized by various melt growth methods such as floating zone,[9)] Czochralski,[10,11)] edge-defined film-fed growth,[12)] vertical Bridgman,[13,14)] and crucible-less bulk melt growth.[15)] These physical properties suggest the great potential of $\beta$-$Ga_2O_3$ for various applications to power electronics and harsh environment electronics. Taking advantage of the availability of high-quality $\beta$-$Ga_2O_3$ epitaxial substrates, vertical $Ga_2O_3$ FETs and diodes with homoepitaxial drift layers have been energetically developed.[16–24)] From a productivity perspective, there are two representative epitaxial growth techniques suitable for future mass production of $Ga_2O_3$ epitaxial wafers: halide vapor phase epitaxy (HVPE) and metalorganic chemical vapor deposition (MOCVD). HVPE can provide high-quality $Ga_2O_3$ thin films at a high growth rate of over 20 $\mu$m h$^{-1}$[25,26)] and thus has been most commonly used to grow drift layers of vertical $Ga_2O_3$ devices. In contrast, MOCVD growth of $Ga_2O_3$ had been suffering from a severe problem of low growth rate.[27–31)] Furthermore, residual electron densities of typical cold-wall MOCVD-grown unintentionally doped (UID) $Ga_2O_3$ films are on the order of $10^{15}$ cm$^{-3}$ or larger[29,31–36)]; therefore there is still a need for improvement. Recently, Yoshinaga et al. reported high-speed growth of high-purity $Ga_2O_3$ homoepitaxial films by low-pressure hot-wall MOCVD that they newly developed.[37)] It has been confirmed that the structural properties of the MOCVD-grown $Ga_2O_3$ films are as good as those of HVPE-grown ones; however, their electrical properties have never been investigated. In this work, we studied room-temperature electrical properties of UID $Ga_2O_3$ thin films grown by the MOCVD technique.

After hydrofluoric acid (HF) cleaning of Sn-doped $n^+$-$Ga_2O_3$ (010) substrates, 15 $\mu$m-thick UID $Ga_2O_3$ layers were grown on the substrates by the low-pressure hot-wall MOCVD using trimethylgallium as a Ga precursor. The growth rate was 5 $\mu$m h$^{-1}$, and details of the other growth parameters were reported elsewhere.[37)] In cases of as-grown Sn-doped $n$-$Ga_2O_3$ bulk single crystals and HVPE-grown Si-doped $n$-$Ga_2O_3$ films, high-temperature annealing is required to activate doped donors.[12,38)] Therefore, in order to investigate the annealing effect on the electrical properties of the MOCVD-grown UID $Ga_2O_3$ layers, we prepared two types of samples with and without high-temperature annealing. All the other device processes were simultaneously conducted under the same conditions.

Figures 1(a) and 1(b) show a schematic cross-section of $Ga_2O_3$ Schottky barrier diodes (SBDs) fabricated in this work and a photo of the substrate on which the SBDs were fabricated, respectively. Blue circles in Fig. 1(b) indicate the devices used for current density–voltage ($J$–$V$) measurements. For one of the samples, high-temperature annealing was performed at 1150 °C in a purified $N_2$ atmosphere for 60 min prior to the device processing, and the other was as-grown. The SBD fabrication process began with lapping and chemical mechanical polishing (CMP) of the substrate backsides. After the cleaning of the substrates with organic solvent, buffered HF, and piranha solution, Si-ion implantation doping was performed for the backsides to form a 150 nm-deep box profile with a Si density of $5 \times 10^{19}$ cm$^{-3}$, followed by activation annealing at 925 °C in a $N_2$ atmosphere for 20 min.[39,40)] Note that both the CMP process to remove a damaged region and the high-density Si doping are necessary to form low-resistance ohmic contacts on the $Ga_2O_3$ (010) surface. Subsequently, another CMP was performed for the epitaxial layers to ensure surface flatness and remove a surface depletion region formed during the high-temperature annealing.[19)] The epitaxial layer thickness after the CMP was 8–9 $\mu$m. After 60 nm-deep $BCl_3$ reactive ion etching (RIE) of the substrate back surfaces, a Ti(20 nm)/Au(200 nm) metal stack was evaporated on them for ohmic cathode electrodes, followed by rapid thermal annealing at 470 °C in a $N_2$ atmosphere for 1 min.[41)] Finally, circular Schottky anode electrodes composed of Pt(15 nm)/Ti(10 nm)/Au(200 nm) layers were formed on top of the epitaxial layers by liftoff. Anode electrodes with diameters of 200 and 400 $\mu$m were used for $J$–$V$ and capacitance–voltage ($C$–$V$) measurements, respectively.

 

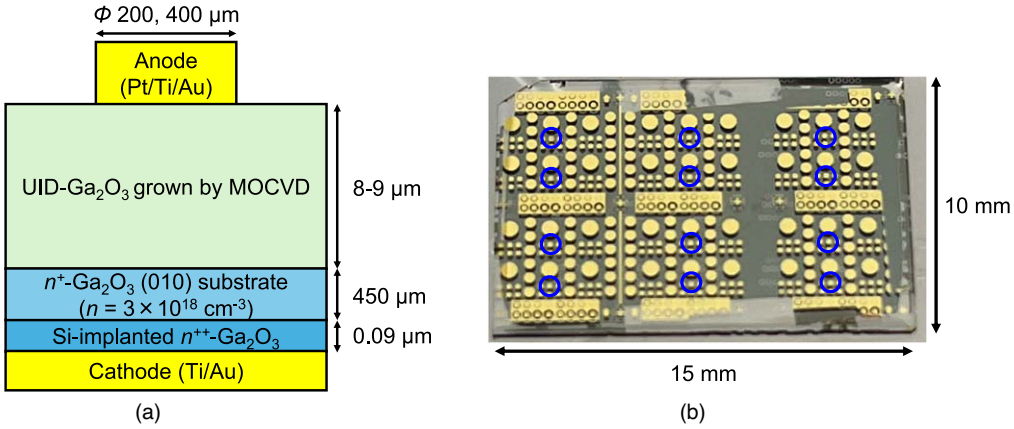


**Fig. 1.** (a) Cross-sectional schematic of $Ga_2O_3$ SBD structure and (b) photo of epitaxial substrate with fabricated SBDs.

Figures 2(a) and 2(b) show the *J*–*V* characteristics of the SBDs fabricated on the annealed and non-annealed $Ga_2O_3$ (010) substrates, respectively. Each figure includes typical characteristics of the SBDs fabricated at a center and an edge part on the substrate. Here, "edge" refers to the area within approximately 3 mm from both the left and right ends of the substrate. All the SBDs exhibited *n*-type diode behavior. When comparing the center- and edge-positioned devices, a significant difference in forward *J* was observed for both annealed and non-annealed substrates. High resistivities of the MOCVD-grown $Ga_2O_3$ thin films were confirmed from large specific on-resistances ($R_{on,sp}$) of the SBDs fabricated at the center parts; the largest $R_{on,sp}$ were $2.2 \times 10^7$ and $4.2 \times 10^6$ Ωcm$^2$ on the annealed and non-annealed substrates, respectively. On the other hand, the SBDs at the edge parts had relatively low $R_{on,sp}$ of 89 and $2.8 \times 10^{-2}$ Ωcm$^2$ on the respective substrates. The in-plane distributions of *J* at $V = +3$ V for the SBDs on the annealed and non-annealed substrates are summarized in Figs. 3(a) and 3(b), respectively, to see resistivity distributions in more detail. With or without the annealing process, the SBDs fabricated at the center part showed extremely low forward *J* of less than $1 \times 10^{-6}$ A cm$^{-2}$, which were at least more than four orders of magnitude lower than those of the SBDs at the edge part. This large difference in forward *J*, i.e., the $R_{on,sp}$ between the center and edge parts was probably due to differences in MOCVD growth parameters such as the substrate temperature and the gas flow rate, which could be caused by fixtures holding four corners of a substrate. It seems that the resistivity was a little increased by the annealing process; however, the causal relationship is still unclear.

Figures 4(a) and 4(b) show the *C*–*V* characteristics of the SBDs fabricated at the center parts on the annealed and non-annealed substrates, respectively. Both SBDs had almost constant *C* regardless of *V*, indicating that the MOCVD-grown UID $Ga_2O_3$ layers were completely depleted over the whole *V* range. From calculations using the mean value of *C* and the relative permittivity of 10.87 in the [010] orientation,[42] residual effective donor densities ($N_d$–$N_a$) of the UID $Ga_2O_3$ layers on both of the annealed and non-annealed substrates were estimated to be less than $3.0 \times 10^{13}$ cm$^{-3}$. Note that the $N_d$–$N_a$ were the lowest for MOCVD-grown homoepitaxial $Ga_2O_3$ films,[29,31–36] and that even the relatively large $N_d$–$N_a$ for the edge devices were still at the level of low $10^{15}$ cm$^{-3}$. These results are qualitatively consistent with the fact that UID Si and C densities in $Ga_2O_3$ layers grown at similar conditions by the same MOCVD reactor were less than the detection limits of the secondary ion mass spectrometry measurement.[37]

Reverse *J*–*V* characteristics of the $Ga_2O_3$ SBDs fabricated on the annealed and non-annealed substrates are shown in Figs. 5(a) and 5(b), respectively. The breakdown measurements were executed using Fluorinert™ to avoid discharging. Both SBDs on the annealed and non-annealed substrates revealed high destructive breakdown voltages of 1.63 and 1.75 kV, respectively. Using thicknesses of the $Ga_2O_3$ epitaxial layers extracted from the *C*–*V* characteristics, the average electric fields in the

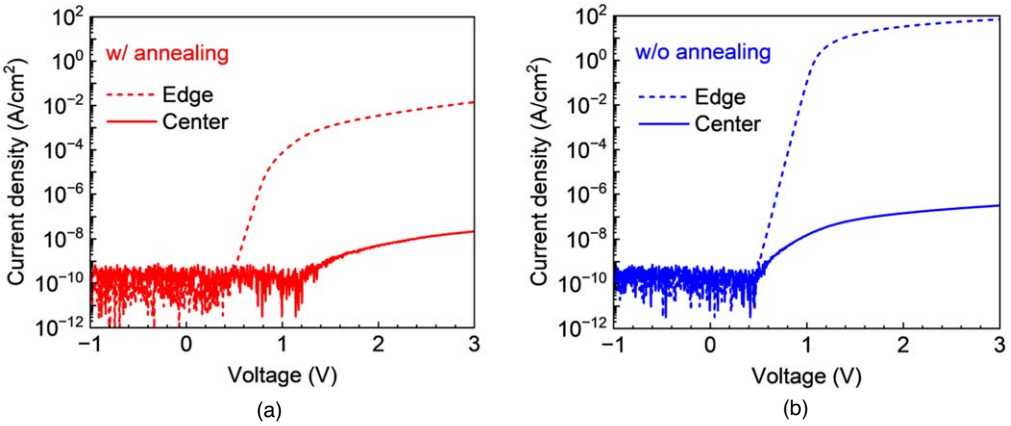


**Fig. 2.** *J*–*V* characteristics of UID $Ga_2O_3$ SBDs fabricated at center and edge parts on (a) annealed and (b) non-annealed epitaxial substrates.

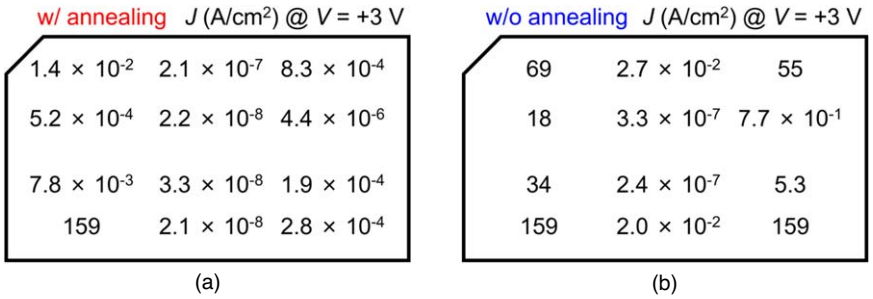


**Fig. 3.** In-plane distribution of $J$ at $V = +3$ V for SBDs fabricated on UID $Ga_2O_3$ layers (a) with and (b) without the annealing process.

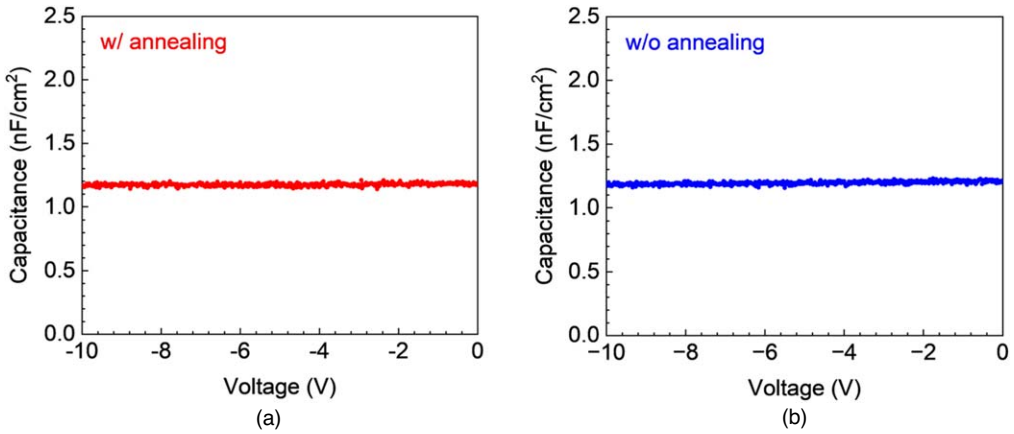


**Fig. 4.** $C$–$V$ characteristics of UID $Ga_2O_3$ SBDs fabricated at center parts on (a) annealed and (b) non-annealed substrates.

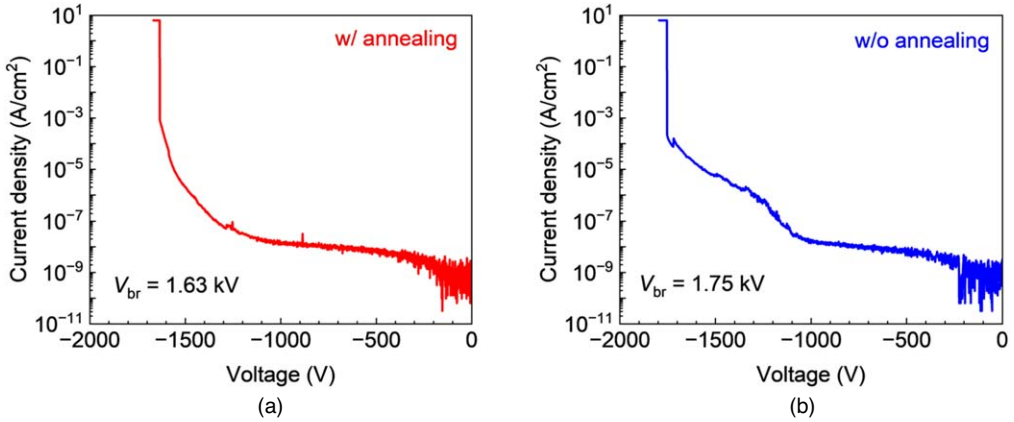


**Fig. 5.** Reverse $J$–$V$ characteristics of UID $Ga_2O_3$ SBDs fabricated at center parts on (a) annealed and (b) non-annealed substrates.

UID $Ga_2O_3$ layers at the breakdown events were estimated to be 2.0 and 2.2 MV cm$^{-1}$ for the annealed and non-annealed epitaxial layers, respectively. These excellent breakdown characteristics of the SBDs without any edge termination can be attributed to the high crystal quality of the MOCVD-grown UID $Ga_2O_3$ layers.

We investigated the electrical properties of UID $Ga_2O_3$ thin films grown by low-pressure hot-wall MOCVD. The UID layers had extremely high resistivities, which were typified by large $R_{on,sp}$ on the order of $10^7$ Ωcm$^2$ or higher for SBDs with them as drift layers. Complete depletion of the UID layers was also confirmed at thermal equilibrium, which corresponded to a $N_d$–$N_a$ of less than $3.0 \times 10^{13}$ cm$^{-3}$. The average electric fields in the UID layers when the destructive breakdown happened were estimated to be ~2 MV cm$^{-1}$. These results indicate that the low-pressure hot-wall MOCVD-grown $Ga_2O_3$ films had highly resistive properties and should be suitable for future device developments.

**Acknowledgments** This work was supported in part by MIC under a grant entitled 'R&D of ICT Priority Technology (JPMI00316): Next-Generation Energy-Efficient Semiconductor Development and Demonstration Project (in collaboration with MOEJ).

**ORCID iDs** Zhenwei Wang https://orcid.org/0000-0002-7834-2591 Junya Yoshinaga https://orcid.org/0009-0002-5892-0419 Takuya Tsutsumi https://orcid.org/0000-0002-5078-606X Yoshinao Kumagai https://orcid.org/0000-0001-8475-9468 Masataka Higashiwaki https://orcid.org/0000-0003-2821-3107

1) T. Onuma, S. Saito, K. Sasaki, T. Masui, T. Yamaguchi, T. Honda, and M. Higashiwaki, Jpn. J. Appl. Phys. **54**, 112601 (2015).
2) M. Higashiwaki and G. H. Jessen, Appl. Phys. Lett. **112**, 060401 (2018).
3) K. Ghosh and U. Singisetti, J. Appl. Phys. **124**, 085707 (2018).
4) Z. Xia et al., Appl. Phys. Lett. **115**, 252104 (2019).

5) K. Sasaki, A. Kuramata, T. Masui, E. G. Víllora, K. Shimamura, and S. Yamakoshi, Appl. Phys. Express **5**, 035502 (2012).
6) M. Baldini, M. Albrecht, A. Fiedler, K. Irmscher, R. Schewski, and G. Wagner, ECS J. Solid State Sci. Technol. **6**, Q3040 (2017).
7) K. Goto, K. Konishi, H. Murakami, Y. Kumagai, B. Monemar, M. Higashiwaki, A. Kuramata, and S. Yamakoshi, Thin Solid Films **666**, 182 (2018).
8) B. J. Baliga, J. Appl. Phys. **53**, 1759 (1982).
9) E. G. Víllora, K. Shimamura, Y. Yoshikawa, K. Aoki, and N. Ichinose, J. Cryst. Growth **270**, 420 (2004).
10) Y. Tomm, P. Reiche, D. Klimm, and T. Fukuda, J. Cryst. Growth **220**, 510 (2000).
11) Z. Galazka, R. Uecker, D. Klimm, K. Irmscher, M. Naumann, M. Pietsch, A. Kwasniewski, R. Bertram, S. Ganschow, and M. Bickermann, ECS J. Solid State Sci. Technol. **6**, Q3007 (2017).
12) A. Kuramata, K. Koshi, S. Watanabe, Y. Yamaoka, T. Masui, and S. Yamakoshi, Jpn. J. Appl. Phys. **55**, 1202A2 (2016).
13) E. Ohba, T. Kobayashi, T. Taishi, and K. Hoshikawa, J. Cryst. Growth **556**, 125990 (2021).
14) Y. Ueda, T. Igarashi, K. Koshi, S. Yamakoshi, K. Sasaki, and A. Kuramata, Jpn. J. Appl. Phys. **62**, SF1006 (2023).
15) A. Yoshikawa, V. Kochurikhin, T. Tomida, I. Takahashi, K. Kamada, Y. Shoji, and K. Kakimoto, Sci. Rep. **14**, 14881 (2024).
16) K. Konishi, K. Goto, H. Murakami, Y. Kumagai, A. Kuramata, S. Yamakoshi, and M. Higashiwaki, Appl. Phys. Lett. **110**, 103506 (2017).
17) Z. Hu, K. Nomoto, W. Li, N. Tanen, K. Sasaki, A. Kuramata, T. Nakamura, D. Jena, and H. G. Xing, IEEE Electron Device Lett. **39**, 869 (2018).
18) W. Li, K. Nomoto, Z. Hu, T. Nakamura, D. Jena, and H. G. Xing, IEDM Tech. Dig.270 (2019).
19) C.-H. Lin et al., IEEE Electron Device Lett. **40**, 1487 (2019).
20) M. H. Wong, H. Murakami, Y. Kumagai, and M. Higashiwaki, IEEE Electron Device Lett. **41**, 296 (2020).
21) F. Otsuka, H. Miyamoto, A. Takatsuka, S. Kunori, K. Sasaki, and A. Kuramata, Appl. Phys. Express **15**, 016501 (2022).
22) S. Kumar, H. Murakami, Y. Kumagai, and M. Higashiwaki, Appl. Phys. Express **15**, 054001 (2022).
23) D. Wakimoto, C.-H. Lin, Q. T. Thieu, H. Miyamoto, K. Sasaki, and A. Kuramata, Appl. Phys. Express **16**, 036503 (2023).
24) S. Roy, B. Kostroun, J. Cooke, Y. Liu, A. Bhattacharyya, C. Peterson, B. Sensale-Rodriguez, and S. Krishnamoorthy, Appl. Phys. Lett. **123**, 243502 (2023).
25) K. Nomura, K. Goto, R. Togashi, H. Murakami, Y. Kumagai, A. Kuramata, S. Yamakoshi, and A. Koukitu, J. Cryst. Growth **405**, 19 (2014).
26) H. Murakami et al., Appl. Phys. Express **8**, 015503 (2015).
27) Z. Feng, A. F. M. A.-U. Bhuiyan, M. R. Karim, and H. Zhao, Appl. Phys. Lett. **114**, 250601 (2019).
28) S. B. Anooz et al., Appl. Phys. Lett. **116**, 182106 (2020).
29) M. J. Tadjer et al., J. Phys. D: Appl. Phys. **54**, 034005 (2021).
30) L. Meng, D. Yu, H.-L. Huang, C. Chae, J. Hwang, and H. Zhao, Cryst. Growth Des. **24**, 3737 (2024).
31) A. Bhattacharyya, C. Peterson, K. Chanchaiworawit, S. Roy, Y. Liu, S. Rebollo, and S. Krishnamoorthy, Appl. Phys. Lett. **124**, 010601 (2024).
32) M. Baldini, M. Albrecht, A. Fiedler, K. Irmscher, D. Klimm, R. Schewski, and G. Wagner, J. Mater. Sci. **51**, 3650 (2016).
33) Y. Zhang, F. Alema, A. Mauze, O. S. Koksaldi, R. Miller, A. Osinsky, and J. S. Speck, APL Mater. **7**, 022506 (2019).
34) F. Alema, Y. Zhang, A. Mauze, T. Itoh, J. S. Speck, B. Hertog, and A. Osinsky, AIP Adv. **10**, 085002 (2020).
35) A. Bhattacharyya, P. Ranga, S. Roy, J. Ogle, L. Whittaker-Brooks, and S. Krishnamoorthy, Appl. Phys. Lett. **117**, 142102 (2020).
36) Z. Feng et al., Phys. Status Solidi RRL **14**, 2000145 (2020).
37) J. Yoshinaga, H. Tozato, T. Okuyama, S. Sasaki, G. Piao, K. Ikenaga, K. Goto, Y. Ban, and Y. Kumagai, Appl. Phys. Express **16**, 095504 (2023).
38) N. T. Son et al., J. Appl. Phys. **120**, 235703 (2016).
39) K. Sasaki, M. Higashiwaki, A. Kuramata, T. Masui, and S. Yamakoshi, Appl. Phys. Express **6**, 086502 (2013).
40) K. R. Gann et al., J. Appl. Phys. **135**, 015302 (2024).
41) M. Higashiwaki, K. Sasaki, T. Kamimura, M. H. Wong, D. Krishnamurthy, A. Kuramata, T. Masui, and S. Yamakoshi, Appl. Phys. Lett. **103**, 123511 (2013).
42) A. Fiedler, R. Schewski, Z. Galazka, and K. Irmscher, ECS J. Solid State Sci. Technol. **8**, Q3083 (2019).